Polyhedron 190 (2020) 114793

Contents lists available at ScienceDirect

Polyhedron

journal homepage: www.elsevier.com/locate/poly

1,3-Bis(1-methyl-1*H*-tetrazol-5-yl)propane and its coordination polymers with Cu_2Cl_4 and Cu_3Cl_6 units

Sergei V. Voitekhovich [a,*], Alexander S. Lyakhov [a], Dmitriy I. Shiman [a], Yuri V. Grigoriev [a], Ludmila S. Ivashkevich [a], Jennifer Klose [b], Berthold Kersting [b], Oleg A. Ivashkevich [a]

[a] Research Institute for Physical Chemical Problems of the Belarusian State University, Leningradskaya 14, 220006 Minsk, Belarus
[b] Institut für Anorganische Chemie, Universität Leipzig, Johannisallee 29, 04103 Leipzig, Germany

ARTICLE INFO

Article history:
Received 23 June 2020
Accepted 26 August 2020
Available online 12 September 2020

Keywords:
Tetrazoles
Copper complexes
Molecular magnetism
X-ray analysis
Coordination polymers

ABSTRACT

1,3-Bis(1-methyl-1*H*-tetrazol-5-yl)propane (bmtp) was prepared by a procedure including regioselective *tert*-butylation of 1,3-bis(1*H*-tetrazol-5-yl)propane and exhaustive methylation of the obtained 1,3-bis(2-*tert*-butyl-1*H*-tetrazol-5-yl)propane, followed by removal of the *tert*-butyl group from the tetrazolium salt under acidic conditions. The ligand bmtp reacts with $CuCl_2{\cdot}2H_2O$ in ethanol to give the complexes $[Cu_3(bmtp)_2Cl_6(H_2O)_2]_n$ and $[Cu(bmtp)Cl_2]_n$. The transformation of $[Cu(bmtp)Cl_2]_n$ into $[Cu_3(bmtp)_2Cl_6(H_2O)_2]_n$ is observed in ethanol. According to single crystal X-ray analysis, $[Cu(bmtp)Cl_2]_n$ was obtained as a mixture of polymorphic forms. They are all 1D coordination polymers, in which polymeric chains include Cu_2Cl_4 units linked to each other by two bridging ligands *via* the tetrazole ring N^4 atoms. $[Cu_3(bmtp)_2Cl_6(H_2O)_2]_n$ presents a 2D coordination polymer, including Cu_3Cl_6 units bonded to four others by ligand molecules. In this complex, the tetrazole ligands show monodentate N^4 and bridging N^3,N^4 coordination. The temperature-dependent magnetic susceptibility measurements of this complex revealed that the copper(II) ions are antiferromagnetically coupled, showing a coupling constant *J* of $-4.0\ cm^{-1}$.

1. Introduction

The design of coordination compounds with multidentate organic ligands bearing a networking ability has represented an active area of research in the chemistry of materials. In this regard tetrazole derivatives offer an excellent class of linkers due to their capability to bridge metal atoms by means of several electron-donating nitrogen atoms of the heterocycle [1–7]. So, tetrazole (**A**, Scheme 1) and its 5-monosubstituted derivatives are often used for the construction of coordination polymers and metal–organic frameworks which are of interest as gas sorbents, catalysts, chemosensors, explosives, luminescent and magnetic materials [7–9]. Under complexation, tetrazoles of this type are usually deprotonated, generating the corresponding anionic tetrazolates (**B**), which act as bridging ligands, showing a wide variety of coordination modes from mono- to tetradentate. Neutral *N*-substituted monotetrazoles of types **C** and **D** rarely show bridging coordination [1–7]. In most complexes, they act as monodentate ligands, coordinated through the tetrazole ring N^4 atom, although examples of coordination by other ring N atoms are also known [10].

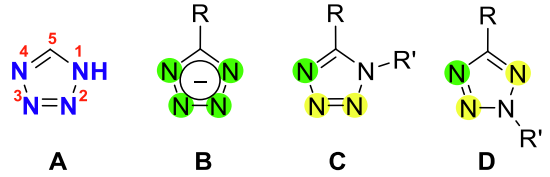

Scheme 1. 1*H*-tetrazole with the ring atom numbering, and some types of tetrazole ligands (main coordination centers are marked in green and rare ones in yellow).

The presence of two tetrazolyl moieties in a molecule gives a potential opportunity to use neutral tetrazoles as coordination linkers. So, N,N-bridged tetrazoles of type **E** (Scheme 2) react with metal salts to generate chain or layered coordination polymers, depending on the nature of the counterion [11–22]. The research interest in their complexes is mainly due to magnetism, spin crossover phenomena and energetic aspects. Because of the different spatial arrangement of the donor centers, C,C-bridged tetrazoles of type **F** have more possibilities for constructing coordination compounds. In contrast to ligands of type **E**, they are able to chelate metal cations, giving mononuclear coordination compounds. Despite this, little attention has been paid to the coordination

* Corresponding author.

https://doi.org/10.1016/j.poly.2020.114793
0277-5387/

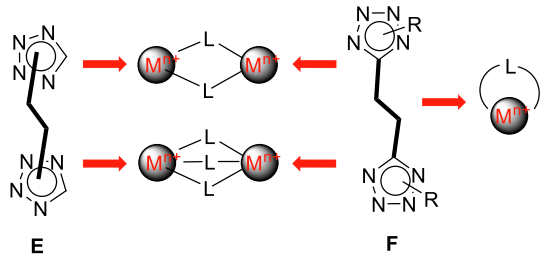

Scheme 2. Some types of bistetrazole ligands (L) and their bridging and chelating coordination motifs.

chemistry of neutral ligands of type **F**. Only a few complexes with such ligands have been reported to date. Transition metal complexes with di(1*H*-tetrazol-5-yl)methane [23], 1,2-di(1*H*-tetrazol-5-yl)ethane [24] and 2,2-di(1*H*-5-tetrazolyl)propane [25] were investigated as energetic materials. In these complexes, the neutral bistetrazoles act as chelating ligands.

1,2-Bis(1-methyl-1*H*-tetrazol-5-yl)ethane was found to show a chelating function, generating a mononuclear complex with copper (II) perchlorate [24], whereas the bridging function of this ligand is realized in a polymeric chain complex with copper(II) chloride [26]. In the latter case, the tetrazole ligand bridges Cu_2Cl_4 units. Such copper halide clusters are of interest as objects for magnetic studies, aimed at finding magneto-structural correlations in Cu(II) polynuclear systems [27,28]. Bistetrazoles are promising ligands for the construction of these clusters. To date, several complexes having Cu_2Cl_4 [29] and rarer Cu_3Cl_6 units [30,31] have been synthesized using *N*-substituted bistetrazoles.

In the present investigation, the novel ligand 1,3-bis(1-methyl-1*H*-tetrazol-5-yl)propane of type **F** was synthesized and its complexation with copper(II) chloride was studied. It was interesting to find out how the elongation of the alkyl bridge compared with that in 1,2-bis(1-methyl-1*H*-tetrazol-5-yl)ethane [26] affects the complexation.

2. Experimental section

2.1. Physical techniques

Elemental analyses for C, H and N were performed on a FlashEA 1112 element analyzer. ^{1}H and ^{13}C NMR spectra were recorded on a Bruker Avance 500 spectrometer. The observed chemical shifts were referenced to solvent signals (δ_H 2.50, δ_c 39.43 ppm). The TG and DSC curves were obtained using a NETZSCH STA 449 F3 thermoanalyzer in a dynamic nitrogen atmosphere (heating rate 10 °C min^{-1}, aluminium oxide, mass 1–3 mg). Infrared spectra were recorded on a Nicolet Thermo Avatar 330 FT–IR system over the 400–4000 cm^{-1} range in SiC cavities. The magnetic properties were investigated by temperature-dependent magnetic susceptibility measurements in the temperature range between 2 and 300 K, in an applied external field of B = μ_0H = 0.5 T, using an MPMS 7XL SQUID magnetometer.

2.2. Synthesis

2.2.1. 1,3-Di(1H-tetrazol-5-yl)propane (**1**)

Triethylammonium chloride (68.8 g, 0.5 mol) and sodium azide (32.5 g, 0.5 mol) were added to a solution of glutaronitrile (21.6 g, 0.23 mol) in toluene (300 ml), and the mixture was stirred at 100–110 °C for 20 h. After cooling the reaction mixture to room temperature, distilled water (250 ml) was added, the aqueous layer was separated and the toluene layer was washed with water (3 × 50 ml). The joint aqueous layers were acidified to pH 2 using conc. hydrochloric acid. The precipitate that formed was filtered off, washed with water and dried in a vacuum oven, giving a white powder. Yield: 96% (39.8 g, 0.22 mol). Mp: 205–210 °C (Lit. 198 °C [32]). ^{1}H NMR (500 MHz, CD_3CN) δ, ppm: 2.25 (quintet, 2H, CH_2), 2.95 (t, 4H, 2 × CH_2). ^{13}C NMR (125 MHz, CD_3CN) δ, ppm: 23.3, 27.5, 155.4 (C_{ring}).

2.2.2. 1,3-Bis(2-tert-butyl-2H-tetrazol-5-yl)propane (**2**)

tert-Butanol (20.0 g, 0.27 mol) was added dropwise with stirring to a solution of 1,3-di(1*H*-tetrazol-5-yl)propane (18.0 g, 0.1 mol) in conc. sulfuric acid (50 ml). The temperature of the reaction mixture should not exceed 30 °C. The mixture was stirred at room temperature for 2.5 h, and then poured on ice (~400 g). The precipitate that formed was filtered off, washed with water and dried *in vacuo*, giving 1,3-bis(2-*tert*-butyl-2*H*-tetrazol-5-yl)propane as a white fine polycrystalline powder. Yield: 95% (27.9 g). Mp: 40–43 °C. ^{1}H NMR (500 MHz, CD_3CN) δ, ppm: 1.66 (s, 18H, 2 × *t*-Bu), 2.19 (quintet, 2H, CH_2), 2.93 (t, 4H, 2 × CH_2). ^{13}C NMR (125 MHz, CD_3CN) δ, ppm: 25.4, 27.1, 29.4, 64.2, 166.3 (C_{ring}).

2.2.3. 1,3-Bis(1-methyl-1H-tetrazol-5-yl)propane (bmtp)

A solution of 1,2-bis(2-*tert*-butyl-1*H*-tetrazol-5-yl)propane (2.39 g, 8.2 mmol) and dimethyl sulfate (2.3 ml, 24.6 mmol) in chloroform (5 ml) was stirred at room temperature for 5 days. Then, hydrochloric acid (36%, 40 ml) was added, and the mixture was stirred for 1 h. The upper aqueous layer of the mixture was separated and heated on a water bath for 5 h. After neutralization of the reaction mixture with sodium hydroxide, the solvent was removed in *vacuo*. The residue was extracted with boiling ethanol and the extract was cooled to 0–5 °C. The precipitate obtained was recrystallized from water to yield colorless crystals of 1,3-bis (1-methyl-1*H*-tetrazol-5-yl)propane. Yield: 65% (1.1 g, 5.3 mmol). Mp: 105–107 °C. ^{1}H NMR (500 MHz, CD_3CN) δ, ppm: 1.60 (quintet, 2H, CH_2), 2.63 (t, 4H, 2 × CH_2), 3.60 (s, 6H, 2 × CH_3). ^{13}C NMR (125 MHz, CD_3CN): δ 22.6, 24.1, 34.0, 155.8 (C_{ring}). IR (cm^{-1}): 2962 s, 2928 m, 1568 w, 1522 s, 1465 s, 1452 s, 1427 s, 1285 s, 1231 m, 1193 m, 1179 m, 1092 m, 1045 m, 1029 m, 976 m, 873 w, 812 m, 755 m, 720 w, 677 s, 646 s, 522 w. $C_7H_{12}N_8$ (208.25): C 40.70 (calc. 40.38); H 5.51 (5.81); N, 53.42 (53.81) %.

2.2.4. Complexation of 1,3-bis(1-methyl-1H-tetrazol-5-yl)propane with copper(II) chloride

A solution of $CuCl_2{\cdot}2H_2O$ (0.34 g, 2 mmol) and bmtp (0.21 g, 1 mmol) in ethanol (50 ml) was allowed to stand at room temperature. After 1 day, the formation of a blue mixture of the polymorphs **Ia** and **Ib** of $[Cu(bmtp)Cl_2]_n$ was observed. Over the next 2 days, these blue polymorphs were transformed into the green complex $[Cu_3(bmtp)_2Cl_6(H_2O)_2]_n$ (**II**). Yield: 70% (0.30 g, 0.35 mol). IR (cm^{-1}): 3555 s, 3443 s, 3153 m, 3032 s, 3008 s, 2991 s, 2966 s, 2863 m, 1590 s, 1528 s, 1480 s, 1446 s, 1412 m, 1369 m, 1338 m1323 m, 1307 m, 1284 m, 1251 m, 1234 m, 1210 m, 1152 m, 1118 m, 1095 m, 1056 s, 1042 m, 994 w, 809 m, 775 m, 721 m, 709 m, 680 m, 659 m, 571 m, 495 m. $C_{14}H_{28}Cl_6Cu_3N_{16}O_2$ (855.84): C 19.75 (calc. 19.65); H 3.43 (3.30); N 25.89 (26.19) %.

A mixture of polymorphs **Ia** and **Ib** was also obtained by heating a solution of $CuCl_2{\cdot}2H_2O$ (0.51 g, 3 mmol) and bmtp (0.42 g, 2 mmol) in ethanol (50 ml) for 10 min at 50–60 °C. The precipitate thus prepared was filtered off and dried in a vacuum oven, giving a mixture of the polymorphs. Yield: 90% (0.61 g, 1.8 mol).

2.3. X-ray structure determination

Single crystal X-ray diffraction data of the ligand bmtp and complexes **Ia**, **Ib**, **Ic** and **II** were collected on a SMART Apex II diffractometer using graphite monochromated Mo-Kα radiation

(λ = 0.71073 Å). The structures were solved by direct methods (SIR2014) [33] and refined on F^2 by the full-matrix least squares technique (SHELXL 2014) [34]. The intensities were corrected for absorption. For all the compounds, non-hydrogen atoms were refined anisotropically. The water hydrogen atoms of complex **II** were determined from the difference Fourier map and refined in an isotropic approximation. All other H atoms of the investigated compounds were placed in calculated positions and refined in a "riding" model, with $U_{iso}(H) = 1.5U_{eq}(C)$ for the methyl groups and $U_{iso}(H) = 1.2U_{eq}(C)$ for the methylene groups. The molecular graphics were performed with the programs ORTEP-3 for Windows [35] and PLATON [36]. Room temperature X-ray powder diffraction data of the obtained blue polycrystalline sample (the mixture of polymorphs **Ia** and **Ib**, Fig. S4) and of the green polycrystalline sample (complex **II**, Fig. S5) were used to control their phase composition. The powder patterns were recorded with an EMPYREAN diffractometer (PANalytical, Netherlands) using Cu-Ka radiation (Ni-filter) at 296 K. CCDC deposition numbers for the compounds are as follows: 2,002,407 (bmtp, 180 K), 2,002,404 (bmtp, 296 K), 2,002,401 (**Ia**, 100 K), 2,002,403 (**Ia**, 296 K), 2,002,402 (**Ib**, 296 K), 2,002,405 (**Ic**, 100 K), 2,002,408 (**II**, 296 K), 2,002,406 (**II**, 100 K).

3. Results and discussion

3.1. Synthesis of the ligand bmtp and its complexation

N-Substituted tetrazoles are frequently synthesized by alkylation of the corresponding 5-monosubstituted tetrazoles. However, in most cases this simple approach has low regioselectivity and, as a consequence, subsequent separation of N^1- and N^2-isomers is required. In the case of bistetrazoles, the number of isomers increases to three, making their separation difficult. Previously, we elaborated a regioselective route to N^1-methyl substituted arylene- [37] and alkylene-bridged bistetrazoles *via* tetrazolium salts [26,38]. Here we successfully applied this approach for the preparation of 1,3-bis(1-methyl-1*H*-tetrazol-5-yl)propane (bmtp). The compound was obtained in a four-step synthesis from glutaronitrile (Scheme 3).

In the first stage of the synthesis, the transformation of the nitrile group into a tetrazol-5-yl one was carried out using an adapted Koguro procedure [39], based on the reaction of nitrile with sodium azide and triethylammonium chloride under reflux in toluene. The advantage of this process is its experimental simplicity, including the product isolation. The initially formed triethylammonium tetrazolate is extracted straight from the reaction mixture into water. Subsequent acidification leads to 1,3-di(1*H*-tetrazol-5-yl)propane (1), which is insoluble in water and easily separated by filtration in 96% yield. The alkylation of **1** was carried out by the action of *tert*-butyl alcohol in concentrated sulfuric acid. It proceeds regioselectively on the N^2 atoms of both tetrazole rings leading to the formation of 1,3-bis(2-*tert*-butyl-2*H*-tetrazol-5-yl)propane (**2**) in 95% yield. The regioselectivity of the alkylation is explained by the protonation of the tetrazole ring at the N^4 atom, resulting in the formation of tetrazolium cations, in which only equivalent N^2 and N^3 atoms are accessible for attack by the carbenium cations generated from the alcohol [37,38]. Further, exhaustive methylation of **2** with dimethyl sulfate gives the tetrazolium salt **3**, which losses the *tert*-butyl group under reflux in acidic conditions, finally leading to the target ligand bmpt.

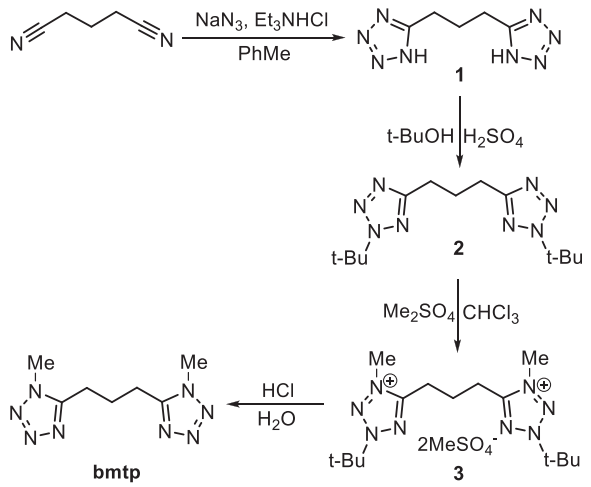

Scheme 3. Preparation of 1,3-bis(1-methyl-1*H*-tetrazol-5-yl)propane (bmtp).

The intermediate **2** and ligand bmtp were attributed to 2,5- and 1,5-disubstituted tetrazoles, correspondingly, based on the ^{13}C NMR chemical shifts of the tetrazole ring C^5 atom. These shifts correspond to well-known literature data of dialkyltetrazoles, whereby the ^{13}C NMR chemical shifts of the C^5 atoms for 2,5-disubstituted tetrazoles are displaced to a low weak field by ~10 ppm in comparison with those of isomeric 1,5-disubstituted tetrazoles [40]. X-ray single crystal analysis of bmtp confirmed the spectral identification.

Complexation of the bistetrazole bmpt with cupric chloride dihydrate was carried out in ethanol (Scheme 4). A solution of the metal salt and ligand was allowed to stand at ambient temperature in the open air and one day later blue crystals were observed. Within the next two days, these crystals, being in the reaction medium, turned green. Note that the blue crystals, being isolated from the reaction medium, are stable. The blue and green crystals were directly picked from the reaction mixtures and investigated by single crystals X-ray analysis. The structural analysis showed that blue crystals had the composition $[Cu(bmtp)Cl_2]_n$ (complex **I**), being present at room temperature in two polymorphic forms (hereinafter referred to as polymorphic forms **Ia** and **Ib**). The same mixture was formed under interaction of the reagents in ethanol at 50–60 °C. The above mentioned green crystals were identified by single crystal X-ray analysis as $[Cu_3(bmtp)_2Cl_6(H_2O)_2]_n$ (complex **II**). Room temperature X-ray powder diffraction of the blue polycrystalline sample confirmed the presence of both **Ia** and **Ib** crystal forms (Fig. S4). Only complex **II** was found in the green polycrystalline sample using powder XRD data (Fig. S5).

Thermal analyses of bmtp and complex **II** were performed from room temperature to 500 °C to examine their thermal stability. The TG and DSC curves of the compounds are presented in Figs. S1–S2. The free ligand shows surprisingly high thermal stability. It forms a melt at 105–107 °C, which shows no decomposition when heated to ~300 °C. Its decomposition begins at ~340 °C, causing an exothermic peak at 371 °C. Complex **II** begins to decompose at the lower temperature of 139 °C, showing an endothermic peak, most probably attributed to the loss of coordinated water molecules. The observed 4.6% weight loss in the TG curve is in good

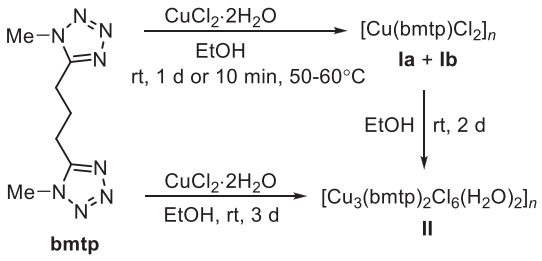

Scheme 4. Complexation of 1,3-bis(1-methyl-1*H*-tetrazol-5-yl)propane with cupric chloride.

agreement with the calculated water content of 4.2%. Further, the dehydrated product was observed to melt and decompose, with endo- and exothermic peaks at 258 and 267 °C, respectively.

3.2. Crystal structure of bmtp and complexes **Ia**, **Ib**, **Ic** and **II**

Crystal data, data collection and structure refinement details for the investigated compounds are summarized in Tables 1 and S1.

3.2.1. Ligand (bmtp)

X-ray single crystal data of bmtp were collected at the temperatures 296 and 180 K. Our attempts to carry out low temperature data collection at 100 K failed because the crystals were destroyed at temperatures lower than 180 K (−93 °C). To understand the reason for such behavior of the bmtp crystals, we performed a low-temperature DSC investigation of the compound from −160 to 20 °C in the temperature rise mode (See Fig. S3). The investigation revealed a reversible structural transition of bmtp at approximately −80 °C, followed by endothermic effect. This temperature is higher in comparison with the above value of −93 °C, below which the destruction of the crystal was observed. A comparison of the obtained main crystal data of bmtp at 180 K (Table 1) and 296 K (Table S1) allowed us to believe that the observed transition takes place between monoclinic and orthorhombic polymorphic forms of bmtp, because lowering the temperature leads to a decrease in the monoclinic angle β to a value very close to 90°. The difference between the transition temperatures, observed in the X-ray and low-temperature DSC investigations, can be explained by thermal hysteresis for the temperature lowering mode (X-ray experiment) and temperature rising mode (low-temperature DSC experiment). The crystal destruction at low temperatures makes it impossible to investigate its orthorhombic form by using single crystal X-ray diffraction. Therefore, here we present only the monoclinic form of bmtp. A detailed description of the structure at 180 K is presented below and the main crystal data at room-temperature are given in Table S1.

The compound crystallizes in the monoclinic space group $P2_1/m$, with two molecules in the unit cell. The asymmetric unit of the compound includes one molecule, shown in Fig. 1. All non-hydrogen atoms of the molecule are located in the crystallographic

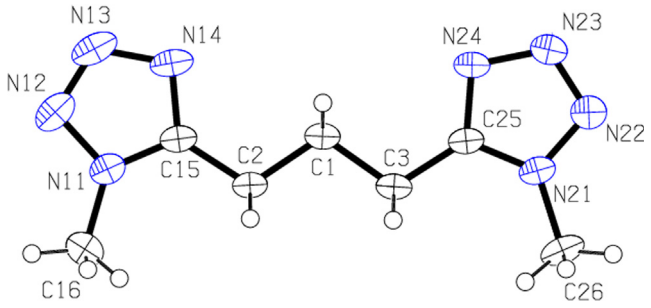

Fig. 1. The molecular structure of bmtp, with displacement ellipsoids drawn at the 50% probability level for non-H atoms. The hydrogen atoms are shown as spheres of arbitrary radii. Disordered methyl H atoms are shown in one position.

mirror plane. The hydrogen atoms of both methyl groups are disordered over two positions with occupancies of 0.5. The non-hydrogen skeleton of the molecule has close to C_{2v} symmetry, with the r.m.s. deviation of non-hydrogen atoms from symmetric positions being 0.017 Å. Bond lengths and valence angles in the molecule show their usual values.

There are no hydrogen bonds in the crystal structure of bmtp, and only π-π stacking interactions take place between the tetrazole rings of neighboring molecules. The interactions between the tetrazole ring N11/C15 at (x, y, z) and the same ring at ($1 - x$, $-½ + y$, $-z$) show an intercentroid distance Cg···Cg of 3.3632(1) Å. The interactions between the ring N21/C25 at (x, y, z) and the same ring at ($-x$, $-½ + y$, $1 - z$) have Cg···Cg distance of 3.4442 (2) Å. The dihedral angle between the rings is equal to 0°. These weak interactions are shown in Fig. 2.

3.2.2. Polymorphs **Ia**, **Ib** and **Ic** of $[Cu(bmtp)Cl_2]_n$

As was mentioned in the previous section, the complex of this composition was obtained at room temperature in two crystal forms, **Ia** and **Ib**. It was found that form **Ia** does not undergo any transitions in the temperature range 100–296 K, thereby we present a detailed structure description of **Ia** for 100 K, and only main crystal data are given for the room temperature structure (Table S1). With regards to the polymorphic form **Ib**, it shows

Table 1
Single crystal X-ray data and structure refinement details for the free ligand bmtp and complexes **Ia**, **Ib**, **Ic** and **II**.

	Bmtp	Complex **Ia**	Complex **Ib**	Complex **Ic**	Complex **II**
Empirical formula	$C_7H_{12}N_8$	$C_7H_{12}Cl_2CuN_8$	$C_7H_{12}Cl_2CuN_8$	$C_{21}H_{36}Cl_6Cu_3N_{24}$	$C_{14}H_{28}Cl_6Cu_3N_{16}O_2$
Formula weight	208.25	342.69	342.69	1028.06	855.84
Temperature (K)	180(2)	100(2)	296(2)	100(2)	100(2)
Crystal system	Monoclinic	Triclinic	Triclinic	Triclinic	Monoclinic
Space group	$P2_1/m$	$P\bar{1}$	$P\bar{1}$	$P\bar{1}$	$P2_1/n$
a (Å)	6.93060(10)	7.43370(10)	7.66750(10)	9.1018(2)	8.96290(10)
b (Å)	6.61160(10)	9.3344(2)	9.1649(2)	11.0414(3)	10.39770(10)
c (Å)	11.2555(2)	10.1387(2)	10.5074(2)	20.8038(5)	15.1566(2)
α (°)	90	86.3716(3)	99.6052(10)	93.3407(11)	90
β (°)	90.0399(5)	70.9586(3)	106.3186(10)	101.2282(12)	93.7106(3)
γ (°)	90	67.7676(3)	111.5753(9)	114.1067(11)	90
V (Å^3)	515.753(14)	614.13(2)	628.06(2)	1849.54(8)	1409.54(3)
Z	2	2	2	2	2
d_c (g cm^{-3})	1.341	1.853	1.812	1.846	2.016
μ (mm^{-1})	0.095	2.208	2.159	2.200	2.861
Crystal size (mm)	0.37 × 0.20 × 0.15	0.23 × 0.18 × 0.14	0.26 × 0.18 × 0.07	0.29 × 0.27 × 0.08	0.26 × 0.23 × 0.08
Reflections collected	19,621	26,012	14,450	46,330	60,405
Independent reflections	2232	3759	3846	12,300	6838
Restraints	0	0	0	0	3
Parameters	93	165	165	493	195
Goodness-of-fit on F^2	1.029	1.036	1.058	1.042	1.082
R1/wR2 [I > 2σ(I)]	0.0435/0.1216	0.0160/0.0427	0.0289/0.0758	0.0208/0.0580	0.0162/0.0396
R1/wR2 [all data]	0.0529/0.1317	0.0166/0.0430	0.0347/0.0793	0.0235/0.0596	0.0181/0.0403
# CCDC	2,002,407	2,002,401	2,002,402	2,002,405	2,002,406

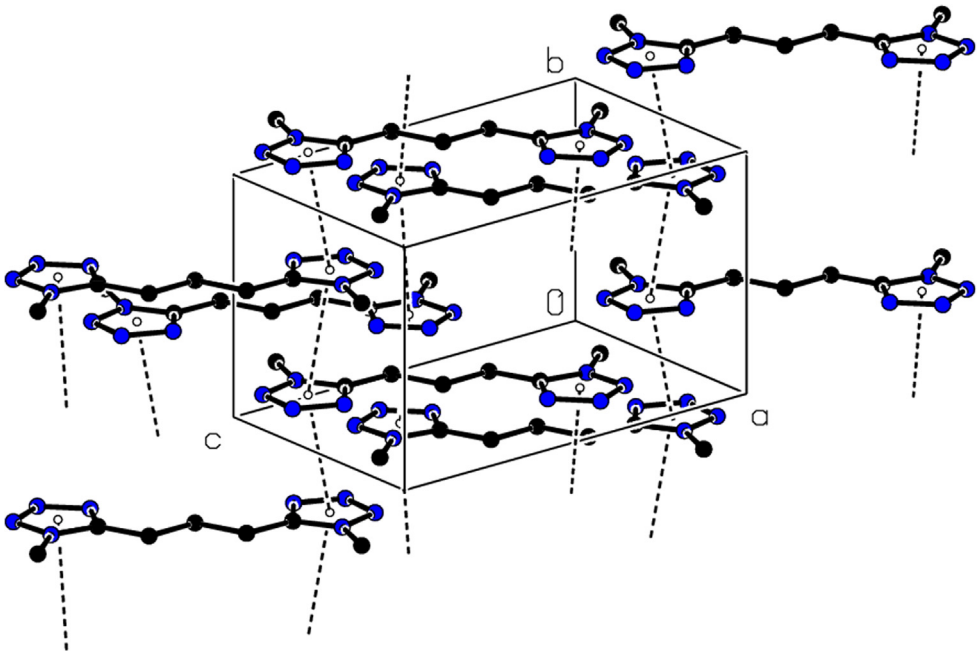

Fig. 2. Crystal packing of bmtp, showing π-π stacking interactions (dashed lines) between the tetrazole rings. Hydrogen atoms are omitted for clarity.

different structures at 100 and 296 K, and therefore descriptions of the structures are given for both temperatures. Because the three polymorphic forms reveal structural similarity in many aspects, first we will describe form **Ia** in detail and then the two other forms will be presented in comparison with form **Ia**.

Polymorph **Ia** crystallizes in the triclinic space group $P\bar{1}$, with two formula units in the unit cell. The asymmetric unit of the compound includes one ligand, one copper atom (Cu1) and two chlorine atoms (Cl1 and Cl2), as shown in Fig. 3. All the atoms occupy general positions. The form **Ia** presents a 1D coordination polymer, with ribbon-like polymeric chains running along the *a* axis (Fig. 4). The chain includes Cu_2Cl_4 units linked together by ligand molecules. Two neighboring Cu_2Cl_4 units in the chain are bonded by two molecules at the expense of the tetrazole ring N^4 atoms. The copper atom shows a distorted square pyramidal coordination, with a τ descriptor for penta-coordination [41] of 0.08.

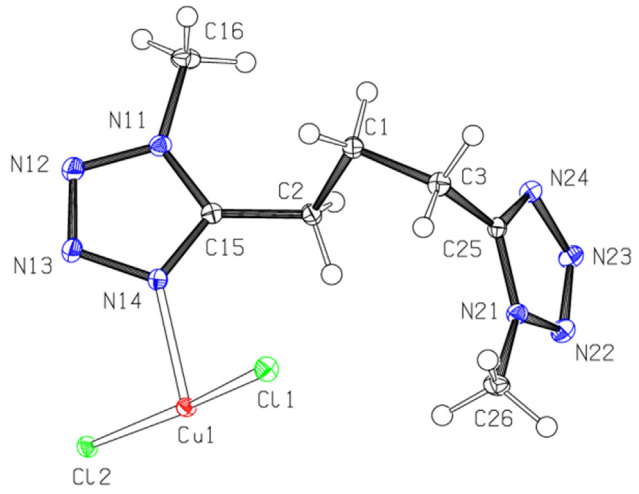

Fig. 3. The asymmetric unit of polymorph **Ia**, with displacement ellipsoids drawn at the 50% probability level for non-H atoms. The hydrogen atoms are shown as spheres of arbitrary radii.

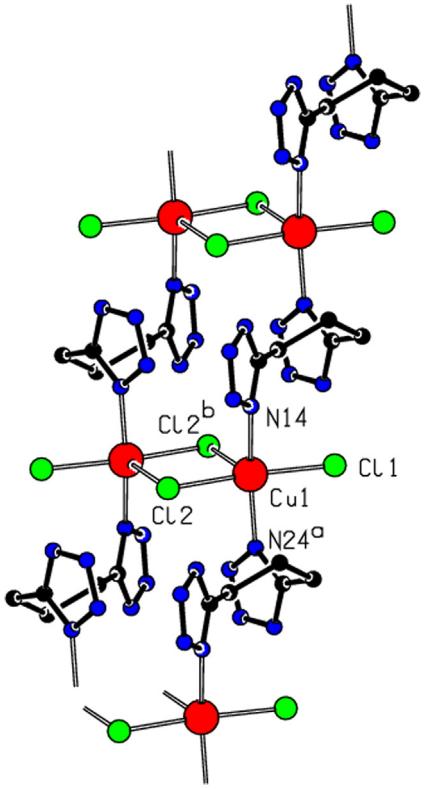

Fig. 4. Fragment of the polymeric chain in the crystal structure of polymorph **Ia**, with the atom labels for the coordination environment of the Cu1 atom. All hydrogen atoms and the methyl groups are omitted for clarity. Symmetry codes: (a) $x-1, y, z$; (b) $-x, 1-y, 1-z$.

The basal sites of the Cu1 pyramid are occupied by two atoms, Cl1 and Cl2, in *trans* positions and by the tetrazole ring atoms N14 and $N24^a$ of two ligands (Fig. 4). The $Cl2^b$ atom lies in the apical site. Symmetry codes (a) and (b) correspond to those in Fig. 4.

Table 2
Coordination bond lengths (Å) in the polymorphic form **Ia** [Symmetry codes (a) and (b) as in Fig. 4].

Cu1–N14	2.0023(8)
Cu1–N24[a]	2.0007(8)
Cu1–Cl1	2.2882(2)
Cu1–Cl2	2.3192(2)
Cu1–Cl2[b]	2.6930(2)

The coordination bond lengths of **Ia** are given in Table 2. The basal bonds are usual in length, whereas the apical bond is elongated. Square pyramids of two symmetry related Cu atoms share an edge so that the apical Cl atom in one pyramid lies in the equatorial site of the other one. The Cu_2Cl_4 unit is centrosymmetric, being composed of the atoms Cu1, Cl1, Cl2 and the symmetry related atoms Cu1[b], Cl1[b] and Cl2[b] [symmetry code (b) correspond to that in Fig. 4]. The Cu1–Cl2–Cu1[b] bridge shows an angle of 93.163(8)°, and the Cu1···Cu1[b] separation is 3.6497(3) Å. The Cu_2Cl_4 unit is rather planar, with a r.m.s. deviation of its atoms from the l.s. plane of 0.0078(1) Å.

In the crystal structure of polymorph **Ia**, there are non-classical hydrogen bonds (C–H···Cl) involving the methylene H atoms. The C2–H2A···Cl2[c] bonds [hydrogen bond geometry: D···A = 3.6545 (11) Å, D–H···A = 154°; symmetry code: (c) 1 + *x*, *y*, *z*] as well as bifurcated C2–H2B···Cl1 [D···A = 3.4386(11) Å, D–H···A = 124°] and C2–H2B···Cl2[b] [D···A = 3.4156(9) Å, D–H···A = 127°] bonds exist inside the coordination chains. C1–H1B···Cl1[d] [D···A = 3.7192(10) Å, D–H···A = 152°; (d) −*x*, 1 − *y*, 2 − *z*] bonds link the polymeric chains into layers parallel to the *ac* plane (Fig. 5).

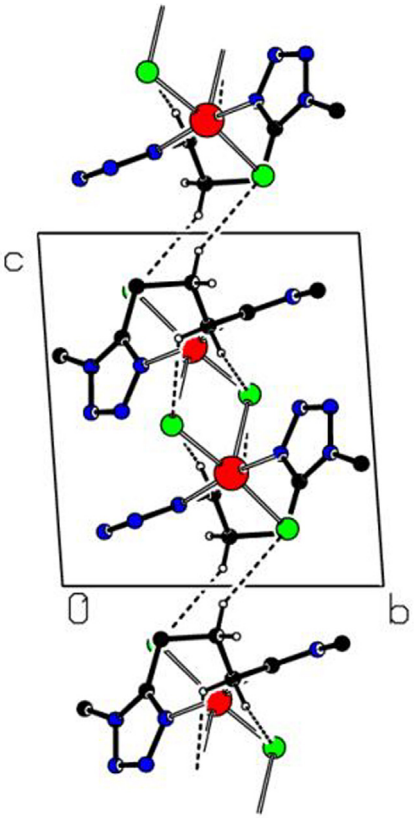

Fig. 5. Crystal packing of the polymorph **Ia** viewed along the *a* axis. Dashed lines show hydrogen bonds. All hydrogen atoms, except for those participating in hydrogen bonds, are omitted for clarity.

Similar to form **Ia**, the polymorphic forms **Ib** and **Ic** are 1D coordination polymers, crystallizing in the same space group $P\bar{1}$. The structural organization of the coordination chains in these forms is very close to that in form **Ia**, as can be seen in Fig. 6, where all the chains are shown in the same manner (they are viewed along the line connecting two bridging chlorine atoms in the Cu_2Cl_4 unit). The conformations of the bridging ligand molecules are also similar in all three polymorphs. The unit cell dimensions of forms **Ia** and **Ib** are close, whereas form **Ic** shows a triple unit cell volume in comparison with the two other forms. The asymmetric units of forms **Ia** and **Ib** are the same, but the asymmetric unit of **Ic** is triple compared to them and includes three independent Cu atoms, six Cl atoms and three ligand molecules. As a result, a longer repeating unit along the coordination chain takes place in form **Ic** (this can be seen in Fig. 6 when looking at the chain in detail).

Fig. 7 allows the difference in the arrangement of the coordination chains in the three polymorphs to be seen. By comparing forms **Ia** and **Ib**, we can select rows of neighboring polymeric chains along the *b* axis. As can be seen, the offset of neighboring rows along the *b* axis is different in the two polymorphs. Also by comparing forms **Ib** and **Ic**, we see the same arrangement of coordination chains, but form **Ic** shows a triple repeating unit along the coordination chain. Figs. S6 and S7, showing precession images for **Ib** and **Ic**, confirming that these complexes present different polymorphic forms.

The coordination polyhedra and coordination bonds in forms **Ib** and **Ic** are close to those in form **Ia** (Table 3). As for the hydrogen bonds in the polymorphic forms, all they show non-classic hydrogen bonds for the methylene H atoms of the type C–H···Cl. In form **Ib**, they occur only inside the coordination chains. In forms **Ia** and **Ic**, there are also inter-chain hydrogen bonds linking coordination chains into layers parallel to the *ac* plane in form **Ia** and to the plane (0 1 −1) in form **Ic**.

3.2.3. Complex **II** $[Cu_3(bmtp)_2Cl_6(H_2O)_2]_n$

This complex crystallizes in the monoclinic space group $P2_1/n$, with two formula units in the unit cell. The asymmetric unit of **II** (Fig. 8) includes two copper atoms (Cu1 and Cu2), three chlorine atoms (Cl1, Cl2 and Cl3), one bmtp ligand and one coordinated water molecule (O1W). The Cu2 atom lies on an inversion center, whereas all other atoms are in general positions.

In complex **II**, the Cu1 and Cu2 atoms show a distorted octahedral coordination (Fig. 9, Table 4). The coordination environment of the Cu1 atom includes two tetrazole ring N^4 atoms (N14 and N24[a]) of two ligand molecules, bridging chlorine atoms (Cl1 and Cl3[a]), a non-bridging chlorine atom (Cl2) and a coordinated water oxygen atom (O1W). The rather long Cu1–Cl3[a] bond of 3.1166(4) Å should be considered as electrostatic in nature. The Cu2 atom is surrounded by two tetrazole ring N^3 atoms (N23 and N23[b]) of two ligands and four bridging chlorine atoms (Cl3, Cl3[b], Cl1[c] and Cl1[d]). The Cu2–Cl1[c](Cl1[d]) bonds are elongated, whereas all other coordination bonds of the Cu2 atom are usual. All symmetry codes correspond to those in Table 4.

Complex **II** contains centrosymmetric Cu_3Cl_6 units, with the a central Cu2 atom and two terminal atoms, Cu1[c] and Cu1[d] (Fig. 9). The central copper atom is bonded to the terminal ones by double chlorido bridges as well as by N^3–N^4 bridges of the tetrazole rings N21/C25. The Cu–Cl–Cu bridge angles take on the values 81.33(1) (Cu2–Cl3–Cu1[c]) and 87.68(1)° (Cu2–Cl1[c]–Cu1[c]). The Cu···Cu distances between the central and terminal copper atoms are both 3.5685(2) Å. Each Cu_3Cl_6 unit is bonded to four others by means of four bridging ligand molecules, forming 2D coordination layers parallel to the (1 0 −1) plane. A fragment of one such coordination

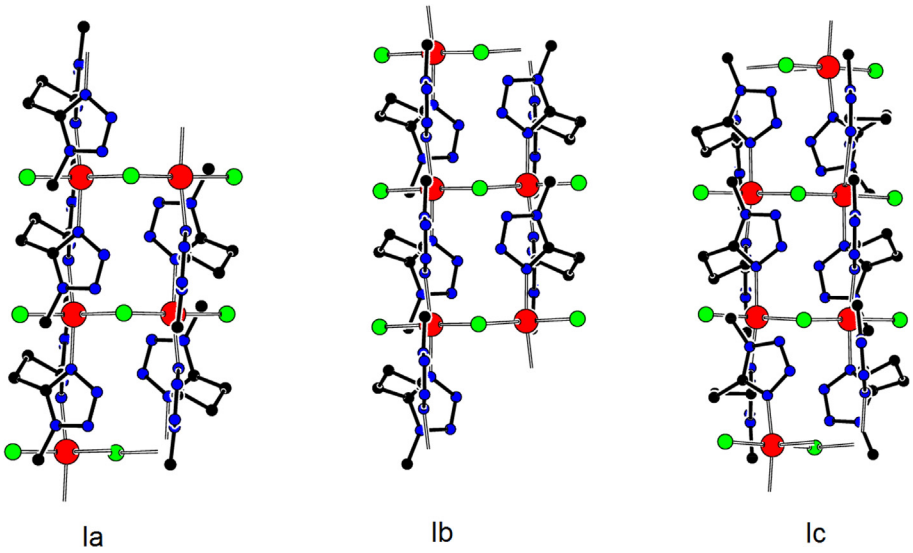

Fig. 6. Fragments of the coordination polymeric chains in polymorphic forms **Ia**, **Ib** and **Ic**. The hydrogen atoms are omitted for clarity.

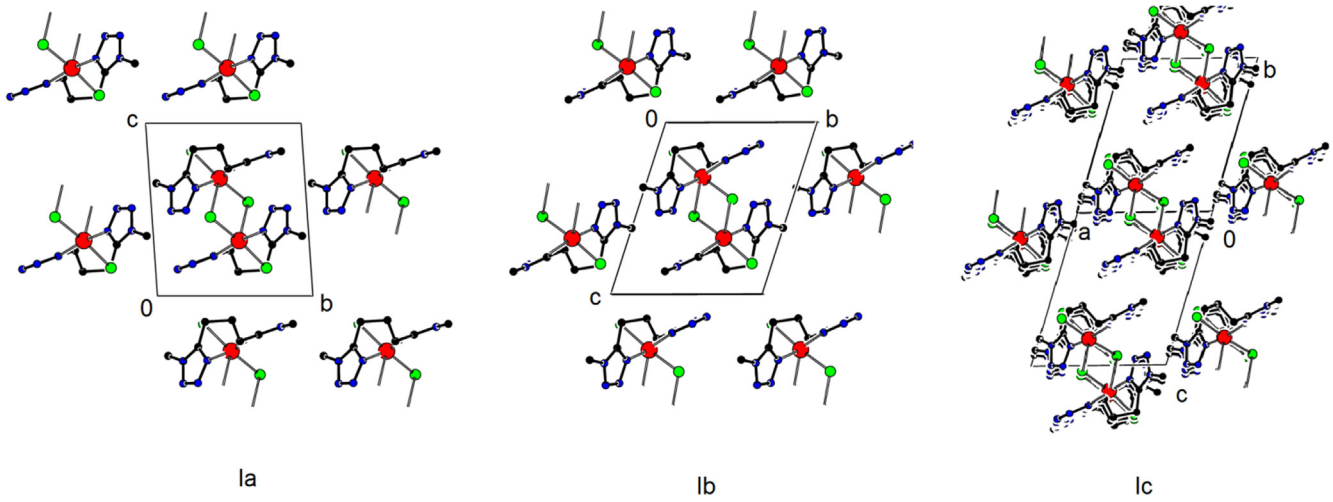

Fig. 7. Crystal packing of the polymorphic forms **Ia**, **Ib** and **Ic** viewed along the coordination chains. In forms **Ia** and **Ib**, the chains extend along the *a* axis, whereas in form **Ic** they run along the vector (***b*** + ***c***). The hydrogen atoms are omitted for clarity.

Table 3
Coordination bond lengths (Å) in the polymorphic forms **Ib** and **Ic**.

Bond	Ib	Ic
Cu–N[4]	2.0049(14), 2.0130(14)	1.9920(8)–2.0209(8)
Cu–Cl(eq)	2.2632(5), 2.3090(4)	2.2540(3)–2.3337(3)
Cu–Cl(ax)	2.7588(5)	2.6531(3)–2.7274(3)

layer is shown in Fig. 10. In the crystal structure of **II**, there are classic O–H···Cl hydrogen bonds for the water H atoms and non-classic C–H···Cl and C–H···O hydrogen bonds for the methylene H atoms, which take place inside the coordination layers and between them (Table 5).

It is of interest to compare the copper(II) chloride complexes of the propylene bridged bistetrazole bmtp with that of the ethylene bridged homologue, 1,2-bis(1-methyl-1*H*-tetrazol-5-yl)ethane (L) [26]. First of all, it is of note that complexation of the ligand L resulted in only one complex, $[CuLCl_2]_n$, whereas two polymorphic forms $[Cu(bmtp)Cl_2]_n$ (**Ia**, **Ib**) and the complex $[Cu_3(bmtp)_2Cl_6(H_2O)_2]_n$ (**II**) were obtained at room temperature in the case of

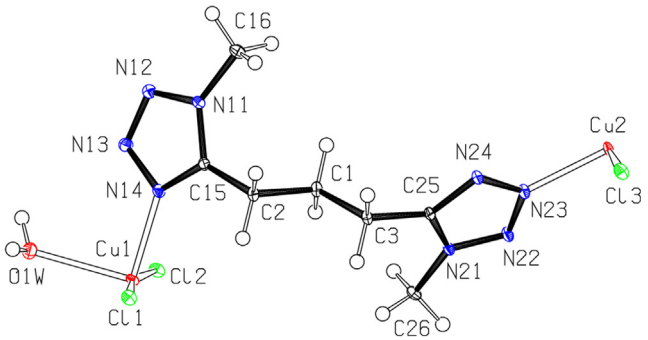

Fig. 8. The asymmetric unit of complex **II**, with displacement ellipsoids drawn at the 50% probability level for non-H atoms. The hydrogen atoms are shown as spheres of arbitrary radii.

bmtp (moreover, one more polymorph, **Ic**, was observed at 100 K). The complexes of both ligands show similar structural features. They are all coordination polymers, namely complexes **Ia-c**

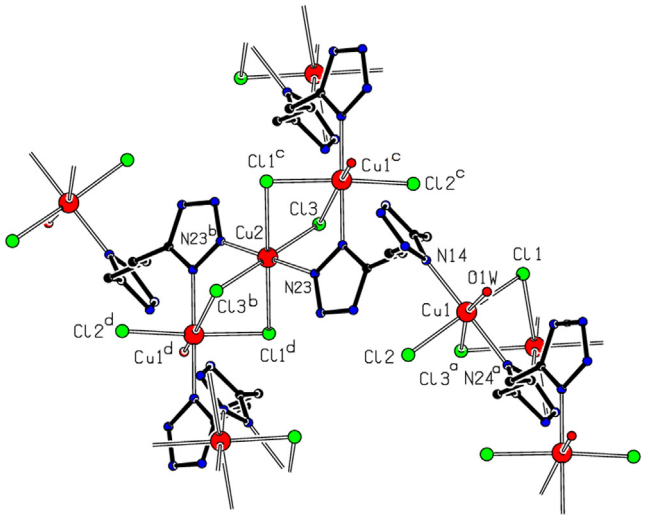

Fig. 9. Structural fragment of complex **II**, showing the coordination environment of the copper atoms. The methyl substituent of the tetrazole ring and all hydrogen atoms are omitted for clarity. Symmetry codes are those as in Table 4.

Table 4
Coordination bond lengths (Å) in complex **II**.

Cu1–N14	2.0114(6)
Cu1–N24^{a}	2.0466(6)
Cu1–Cl2	2.27372(18)
Cu1–Cl1	2.30018(18)
Cu1–O1W	2.3028(6)
Cu1–Cl3^{a}	3.1166(4)
Cu2–N23(N23^{b})	2.0355(6)
Cu2–Cl3(Cl3^{b})	2.27064(16)
Cu2–Cl1^{c}(Cl1^{d})	2.8230(2)

Symmetry codes: (a) −½ + *x*, ½ − *y*, ½ + *z*; (b) 1 − *x*, 1 − *y*, −*z*; (c) ½ + *x*, ½ − *y*, −½ + *z*; (d) ½ − *x*, ½ + *y*, ½ − *z*.

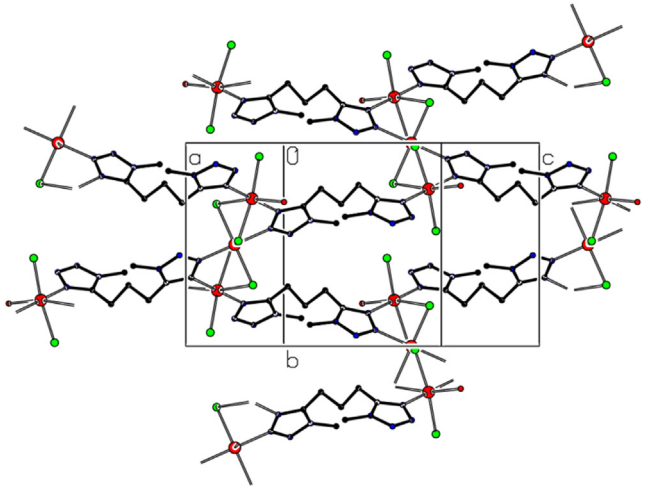

Fig. 10. Coordination polymeric layer, parallel to the (1 0 −1) plane, in the crystal structure of complex **II**. All hydrogen atoms are omitted for clarity.

and $[CuLCl_2]_n$ are 1D polymers, and complex **II** is 2D polymer. They all include either dimeric Cu_2Cl_4 units (**Ia-c** and $[CuLCl_2]_n$) or trimeric Cu_3Cl_6 units (complex $[Cu_3(bmtp)_2Cl_6(H_2O)_2]_n$). These copper-chloride units are linked to each other by bistetrazole ligands

Table 5
Hydrogen bond geometries (Å, °) in the crystal structure of complex **II**.

D–H···*A*	*D*–H	*D*···*A*	*D*–H···*A*
O1W–H1WA···Cl1^{e}	0.812(12)	3.5174(6)	129.8(12)
O1W–H1WA···Cl3^{f}	0.812(12)	3.5879(6)	141.6(12)
O1W–H1WB···Cl2^{g}	0.794(12)	3.2543(6)	174.1(13)
C2–H2A···Cl1	0.99	3.5157(7)	131
C2–H2B···Cl1^{h}	0.99	3.6853(7)	164
C3–H3A···O1W^{c}	0.99	3.1657(9)	116

Symmetry codes: (c) *x* + ½, −*y* + ½, *z* − ½; (e) −*x* + ½, *y* + ½, −*z* + $^{3}/_{2}$; (f) *x*, *y*, *z* + 1; (g) −*x* + ½, *y* − ½, −*z* + $^{3}/_{2}$; (h) −*x* + 1, −*y*, −*z* + 1

to form coordination polymers. However, there are structural differences between the compared complexes. In the 1D coordination polymers **Ia-c** and $[CuLCl_2]_n$, the positions of the bistetrazole ligands relative to the Cu_2Cl_4 planes are different. While the ligand L shows only the $N^4,N^{4'}$-bridging coordination mode, the ligand bmtp additionally reveals the typical monodentate N^4 coordination and also bridging N^3,N^4 coordination, which is rare for 1,5-disubstituted tetrazoles [10]. Taking this into account, it is reasonably to think that elongation of the alkyl bridge makes the ligand more flexible and able to generate a variety of complexes with diverse coordination modes of the ligand.

4. Magnetic properties of complex II

The presence of Cu_3Cl_6 units separated by organic ligands determines the interest for a magnetic investigation of complex **II**. Only two nearby structural analogues of the complex $[Cu_3(bmtp)_2Cl_6(H_2O)_2]_n$ have been found in the literature. These are $Cu_3Cl_6L_4$, where L = 1-allylbenzotriazole [42] and 2-*tert*-butyl-6-([1,2,4]triazolo[4,3-*a*]quinolin-1-yl)phenol) [43]. In the structures of both these complexes, the neighboring Cu^{II} ions are connected by two chlorido bridges and one N–N bridge of a triazole ligand. However, their magnetic properties were not reported.

The magnetic data of polycrystalline complex **II** are shown as a $\mu_{eff}(T)$ curve in Fig. 11. At 300 K, the effective magnetic moment μ_{eff} is 3.39 μB per trinuclear complex, which is higher than the value expected for three non-interacting Cu^{II} cations (S = ½; μ_{eff} = 3.0 μB) and lower than the value expected for three coupled Cu^{II} cations (S = $^{3}/_{2}$; μ_{eff} = 3.87 μB). The μ_{eff} value remains nearly constant on decreasing the temperature down to 70 K. Upon further lowering of the temperature, μ_{eff} rapidly decreases to 2.25 μB at

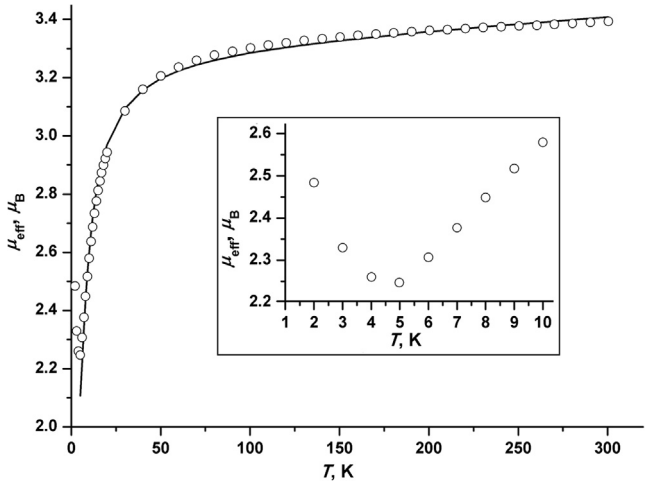

Fig. 11. Temperature dependence of μ_{eff} for **II** per tricopper unit. The solid line represents the best theoretical fit. The insert shows temperature dependence of μ_{eff} at 2–10 K.

5 K. On lowering the temperature even further, μ_{eff} rises to 2.48 μB at 2 K. This behavior implies that the electron spins on the copper ions are coupled by an antiferromagnetic exchange interaction. Antiferromagnetic coupling between the copper ions is also confirmed by the negative Weiss temperature obtained by fitting the reciprocal susceptibility data as $\chi^{-1}(T)$ for complex **II** to the Curie–Weiss law (Fig. S8). Fitting the data for 40–300 K resulted in a Curie constant and Weiss parameter of −7.89 K and 1.47 cm^3 mol^{-1} K, respectively.

The increase in μ_{eff} on cooling below 5 K may originate from weak ferromagnetic interactions between neighboring Cu_3Cl_6 units. These interactions can be provided by two-chloride superexchange pathways [44], because a short Cl···Cl contact of 4.371 Å (room temperature) between the Cu_3Cl_6 units was observed in the crystal structure of **II**. An isothermal analysis of the $M(H)$ curve (Fig. 12) shows that the magnetization has no linear character. At 7 T it reaches value of 1.30 $N\mu_B$, which is more than the value of 1 $N\mu_B$ expected for a tricopper unit having the S = ½ ground state, due to antiferromagnetic exchange interactions between neighboring copper ions. This also can indicate weak ferromagnetic interactions between the Cu_3Cl_6 units at low temperature.

The temperature dependence of the magnetic susceptibility was simulated using the appropriate spin Hamiltonian (Eq. (1)), which includes the isotropic Heisenberg-Dirac-van-Vleck exchange as well as the single-ion Zeeman interactions, using a full-matrix diagonalization approach:

$$\hat{H} = 2\left(-2J_1\hat{S}_1\hat{S}_2\right) + \left(-2J_2\hat{S}_1\hat{S}_3\right) + \mu_B\sum_{i=1}^{3}\left(g\hat{S}_i\hat{B}\right) \quad (1)$$

where J represents the intramolecular magnetic coupling constant, $\hat{S}$ is the Cu spin-vector operator, g is the g-factor, μ_B is the Bohr magneton and B is the applied external magnetic field. The simulation was done using the program "MagProp" [45].

Scheme 5 illustrates the exchange coupling pathways used to model the susceptibility for complex **II**. In this model, the exchange interaction between the neighboring copper ions is represented by J_1, whereas J_2 corresponds to the interaction between the two terminal ions. The g-values were considered to be identical for the three metal ions. A reasonable fit of the experimental susceptibility was possible in the temperature range 5–300 K, which led to J_1 = −4.0 cm^{-1} and g = 2.21 (Fig. 11). The inclusion of the J_2 parameter did not improve the fit and J_2 was fixed at 0 cm^{-1}. It should be noted that fitted g-value slightly differs from the value of 2.29 calculated based on the Curie constant obtained by the fitting of the Curie–Weiss law (Fig. S6).

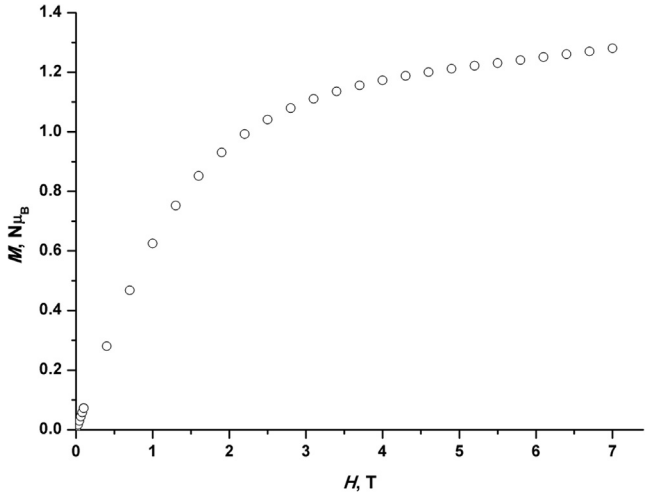

Fig. 12. Isothermal magnetization plots of complex **II** at 2 K.

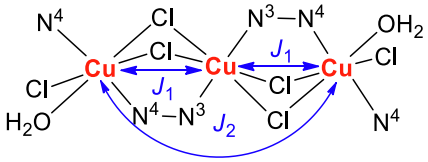

Scheme 5. Magnetic exchange pathways used for simulation of the magnetic susceptibility for the trinuclear subunits in **II**.

5. Conclusion

We have synthesized a novel C,C-propylene bridged bistetrazole ligand and studied its complexation with copper(II) chloride. Like its homologue C,C-ethylene bridged bistetrazole, the studied ligand shows a $N^4,N^{4'}$-bridging coordination mode, giving one-dimensional coordination polymers with Cu_2Cl_4 units. However, these complexes are unstable in solution, transforming to a two-dimensional coordination polymer, which includes trinuclear Cu_3Cl_6 units linked together by bistetrazole ligands. In this complex, the 1,5-disubstituted tetrazole moiety exhibits a rare N^3, N^4-bridging coordination of the hetero-ring. Since the Cu_3Cl_6 units are sufficiently separated from each other by the bistetrazole ligands, preventing electronic interactions between the units, this complex presents an attractive object for molecular magnetism studies of trinuclear systems. The complex was found to exhibit weak antiferromagnetic coupling between the neighboring copper atoms in the trinuclear unit. At low temperature, weak ferromagnetic interactions between these units also take place.

CRediT authorship contribution statement

Sergei V. Voitekhovich: Conceptualization, Investigation, Writing - original draft. **Alexander S. Lyakhov:** Investigation. **Dmitriy I. Shiman:** Investigation. **Yuri V. Grigoriev:** Investigation. **Ludmila S. Ivashkevich:** Writing - original draft. **Jennifer Klose:** Investigation. **Berthold Kersting:** Writing - review & editing. **Oleg A. Ivashkevich:** Supervision.

Declaration of Competing Interest

The authors declare that they have no known competing financial interests or personal relationships that could have appeared to influence the work reported in this paper.

Acknowledgements

This work was supported by Belarusian Republican Foundation for Fundamental Research (grant X18P-043). Dr. Sergei Voitekhovich acknowledges the support of the research fellowship from the Alexander von Humboldt Foundation (Alumni Program).

Appendix A. Supplementary data

Supplementary data to this article can be found online at https://doi.org/10.1016/j.poly.2020.114793.

References

[1] P.N. Gaponik, S.V. Voitekhovich, O.A. Ivashkevich, Russ. Chem. Rev. 75 (2006) 507.
[2] H. Zhao, Z.-R. Qu, H.-Y. Ye, R.-G. Xiong, Chem. Soc. Rev. 37 (2008) 84.

[3] G. Aromi, L.A. Barrios, O. Roubeau, P. Gamez, Coord. Chem. Rev. 255 (2011) 485.
[4] W. Ouellette, S. Jones, J. Zubieta, CrystEngComm 13 (2011) 4457.
[5] E.A. Popova, R.E. Trifonov, V.A. Ostrovskii, ARKIVOC (2012) 45.
[6] M. Massi, S. Stagni, M.I. Ogden, Coord. Chem. Rev. 375 (2018) 164.
[7] A. Tăbăcaru, C. Pettinari, S. Galli, P. Gamez, Coord. Chem. Rev. 372 (2018) 1.
[8] J.-P. Zhang, Y.-B. Zhang, J.-B. Lin, X.-M. Chen, Chem. Rev. 112 (2012) 1001.
[9] K.A. McDonald, S. Seth, A.J. Matzger, Cryst. Growth Des. 15 (2015) 5963.
[10] S.V. Voitekhovich, A.S. Lyakhov, V.E. Matulis, L.S. Ivashkevich, O.A. Ivashkevich, Polyhedron 162 (2019) 100.
[11] J.-G. Xu, X.-Z. Li, H.-F. Wu, F.-K. Zheng, J. Chen, G.-C. Guo, Cryst. Growth Des. 19 (2019) 3934.
[12] M. Ksiazek, M. Weselski, M. Ilczyszyn, J. Kusz, R. Bronisz, Chem. Eur. J. 25 (2019) 2250.
[13] N. Szimhardt, M.H.H. Wurzenberger, T.M. Klapötke, J.T. Lechner, H. Reichherzer, C.C. Unger, J. Stierstorfer, J. Mater. Chem. A 6 (2018) 6565.
[14] M. Weselski, M. Ksiazek, J. Kusz, A. Białońska, D. Paliwoda, M. Hanfland, M.F. Rudolf, Z. Ciunik, R. Bronisz, Eur. J. Inorg. Chem. (2017) 1171.
[15] M. Joas, T.M. Klapötke, Z. Anorg, Allg. Chem. 640 (2014) 1886.
[16] P.-P. Liu, Y.-Q. Wang, C.-Y. Tian, H.-Q. Peng, E.-Q. Gao, J. Mol. Struct. 920 (2009) 459.
[17] R.-Y. Li, B.-W. Wang, X.-Y. Wang, X.-T. Wang, Z.-M. Wang, S. Gao, Inorg. Chem. 48 (2009) 7174.
[18] J.-H. Yu, K. Mereiter, N. Hassan, C. Feldgitscher, W. Linert, Cryst. Growth Des. 8 (2008) 1535.
[19] P.-P. Liu, A.-L. Cheng, N. Liu, W.-W. Sun, E.-Q. Gao, Chem. Mater. 19 (2007) 2724.
[20] P.J. van Koningsbruggen, Y. Garcia, G. Bravic, D. Chasseau, O. Kahn, Inorg. Chim. Acta 326 (2001) 101.
[21] P.J. van Koningsbruggen, Y. Garcia, H. Kooijman, A.L. Spek, J.G. Haasnoot, O. Kahn, J. Linares, E. Codjovi, F. Varret, J. Chem. Soc., Dalton Trans. (2001) 466.
[22] Y. Garcia, P.J. van Koningsbruggen, H. Kooijman, A.L. Spek, J.G. Haasnoot, O. Kahn, Eur. J. Inorg. Chem. (2000) 307.
[23] M. Freis, T.M. Klapötke, J. Stierstorfer, N. Szimhardt, Inorg. Chem. 56 (2017) 7936.
[24] J. Evers, I. Gospodinov, M. Joas, T.M. Klapötke, J. Stierstorfer, Inorg. Chem. 53 (2014) 11749.
[25] N. Szimhardt, M.S. Gruhne, M. Lommel, A. Hess, M.H.H. Wurzenberger, T.M. Klapötke, J. Stierstorfer, Z. Anorg, Allg. Chem. 645 (2019) 354.
[26] D.O. Ivashkevich, A.S. Lyakhov, D.S. Pytleva, S.V. Voitekhovich, P.N. Gaponik, Acta Crystallogr., Sect. C: Cryst. Struct. Commun. 59 (2003) m221.
[27] P. Torres-García, F. Luna-Giles, B. Garcia, C. Platas-Iglesias, D. Esteban-Gómez, E. Vinuelas-Zahinos, New J. Chem. 41 (2017) 8818.
[28] I.M. Grigorieva, T.V. Serebryanskaya, Y.V. Grigoriev, A.S. Lyakhov, L.S. Ivashkevich, A.S. Bogomyakov, L.G. Lavrenova, S.V. Voitekhovich, O.A. Ivashkevich, Polyhedron 151 (2018) 74.
[29] S.V. Voitekhovich, A.P. Mosalkova, A.S. Lyakhov, S. Schmorl, B. Kersting, L.S. Ivashkevich, O.A. Ivashkevich, Z. Anorg, Allg. Chem. 644 (2018) 1611.
[30] H. Gallardo, E. Meyer, A.J. Bortoluzzi, F. Molin, A.S. Mangrich, Inorg. Chim. Acta 357 (2004) 505.
[31] S.V. Voitekhovich, A.S. Lyakhov, L.S. Ivashkevich, S. Schmorl, B. Kersting, O.A. Ivashkevich, Cryst. Growth Des. 17 (2017) 1796–1805.
[32] V.Y. Zubarev, R.E. Trifonov, V.V. Poborchii, V.A. Ostrovskii, Chem. Heterocycl. Compd. 42 (2006) 469.
[33] M.C. Burla, R. Caliandro, B. Carrozzini, G.L. Cascarano, C. Cuocci, C. Giacovazzo, M. Mallamo, A. Mazzone, G. Polidori, J. Appl. Cryst. 48 (2015) 306.
[34] G.M. Sheldrick, Acta Crystallogr. Sect. C: Cryst. Struct. Commun. 71 (2015) 3.
[35] L.J. Farrugia, J. Appl. Crystallogr. 30 (1997) 565.
[36] A.L. Spek, Acta Crystallogr. Sect. D: Biol. Crystallogr. 65 (2009) 148.
[37] S.V. Voitekhovich, P.N. Gaponik, A.S. Lyakhov, Chem. Heterocycl. Compd. 36 (2000) 326.
[38] S.V. Voitekhovich, P.N. Gaponik, D.S. Pytleva, A.S. Lyakhov, O.A. Ivashkevich, Pol. J. Chem. 76 (2002) 1371.
[39] K. Koguro, T. Oga, S. Mitsui, R. Orita, Synthesis (1998) 910.
[40] M. Begrtup, J. Elguero, R. Faure, P. Camps, C. Estopá, D. Ilavský, A. Fruchier, C. Marzin, J. Mendoza, Magn. Reson. Chem. 26 (1988) 134.
[41] A.W. Addison, T.N. Rao, J. Reedijk, J. van Rijn, G.C. Verschoor, J. Chem. Soc., Dalton Trans. (1984) 1349.
[42] E.A. Goreshnik, D. Schollmeyer, M.G. Mys'kiv, Z. Anorg, Allg. Chem. 631 (2005) 8357.
[43] R.F. Brissos, E. Torrents, F.M. dos S. Mello, W.C. Pires, E. de P. Silveira-Lacerda, A.B. Caballero, A. Caubet, C. Massera, O. Roubeau, S.J. Teat, P. Gamez, Metallomics 6 (2014) 1853.
[44] C.P. Landee, M.M. Turnbull, Eur. J. Inorg. Chem. (2013) 2266.
[45] R.T. Azuah, L.R. Kneller, Y. Qiu, P.L.W. Tregenna-Piggott, C.M. Brown, J.R.D. Copley, R.M.J. Dimeo, J. Res. Natl. Inst. Stand. Technol. 114 (2009) 341.